

Pressure-induced superconductivity beyond magnetic quantum criticality in a Kondo ferromagnet

Yanan Zhang,^{1,*} Yongjun Zhang,^{2,*} Jiawen Zhang,^{1,*} Kaixin Ye,¹ Dajun Su,¹ Yanen Huang,¹ Zhaoyang Shan,¹ Jiyuan Li,² Rui Li,¹ Ye Chen,¹ Xin Lu,¹ Lin Jiao,¹ Yu Liu,^{1,†} Michael Smidman,^{1,‡} Frank Steglich,^{1,3} and Huiqiu Yuan^{1,4,5,6,7,§}

¹*New Cornerstone Science Laboratory,
Center for Correlated Matter and School of Physics,
Zhejiang University, Hangzhou 310058, China*

²*Hubei Key Laboratory of Photoelectric Materials and Devices,
School of Materials Science and Engineering,
Hubei Normal University, Huangshi 435002, China*

³*Max Planck Institute for Chemical Physics of Solids (MPI CPfS), 01187 Dresden, Germany*

⁴*Institute of Fundamental and Transdisciplinary Research,
Zhejiang University, Hangzhou 310058, China*

⁵*Institute for Advanced Study in Physics,
Zhejiang University, Hangzhou 310058, China*

⁶*State Key Laboratory of Silicon and Advanced Semiconductor Materials,
Zhejiang University, Hangzhou 310058, China*

⁷*Collaborative Innovation Center of Advanced Microstructures, Nanjing 210093, China*

(Dated: February 11, 2026)

Quantum phase transitions are an established setting for emergent phenomena driven by strong electronic correlations, including strange metals and unconventional superconductivity. These have been explored extensively in Kondo lattice materials tuned to an antiferromagnetic quantum critical point (QCP), but superconductivity emerging near ferromagnetic quantum criticality is not yet observed, and the conditions under which it occurs in proximity to ferromagnetism are undetermined. Here, we report a new setting for superconductivity in the ferromagnetic Kondo-lattice material Ce_5CoGe_2 , where there is a ferromagnetic ground state at ambient pressure, which evolves to antiferromagnetism under applied pressures. The antiferromagnetic transition is suppressed to a zero-temperature QCP, which is accompanied by strange-metal behavior. Superconductivity does not occur at the QCP, but instead appears at pressures beyond the magnetic instability. These findings suggest that Ce_5CoGe_2 represents a distinct class of correlated materials exhibiting a unique scenario for the emergence of superconductivity, likely associated with unconventional pairing mechanisms beyond spin-fluctuations.

The close proximity of unconventional superconductivity to magnetism has been revealed in a variety of materials settings, including heavy-fermion superconductors [1], high-temperature cuprate [2] and iron-based superconductors [3], and organic superconductors [4], which has been interpreted in the framework of the superconductivity being driven by spin fluctuations [5, 6]. This paradigm has been extensively investigated in heavy-fermion antiferromagnets [7–12], where the relative strengths of the competing Ruderman–Kittel–Kasuya–Yosida (RKKY) and Kondo interactions are tuned by experimentally applying non-thermal control parameters, and unconventional superconductivity often emerges upon the suppression of antiferromagnetic order at a QCP. Moreover, in such systems superconductivity may also arise driven by other degrees of freedom, such as quadrupolar [13] or valence fluctuations [14–16], where the latter has been proposed to explain the second superconducting state of pressurized CeCu_2Si_2 , which is well separated from the AFM QCP [14, 17, 18], as illustrated in Fig. 1a.

* These authors contributed equally to this work.

† Corresponding author: liuyuccm@zju.edu.cn

‡ Corresponding author: msmidman@zju.edu.cn

§ Corresponding author: hqyuan@zju.edu.cn

In contrast, the evidence for superconductivity arising from ferromagnetic (FM) quantum criticality is more limited [19]. Although several uranium-based compounds exhibit the coexistence of superconductivity and FM order (Fig. 1b), in these cases the FM transition terminates abruptly under pressure at a first-order transition, avoiding a QCP [20–22]. On the other hand, while pressure and doping have been reported to induce continuous FM QCPs in CeRh_6Ge_4 [23, 24] and $\text{YbNi}_4(\text{P}_{1-x}\text{As}_x)_2$ [25], respectively (Fig. 1c), no superconductivity has yet been found in such materials. Another scenario whereby FM quantum criticality is avoided is by a change of ground state from FM order, to spin-density wave (SDW) or other forms of AFM ground state upon tuning with pressure or doping. Typical examples include the Kondo lattice materials CeRu_2Ge_2 [26], CeAgSb_2 [27] and CeRuPO [28] as well as transition metal compounds NbFe_2 [29] and LaCrGe_3 [30], in which superconductivity is also not yet observed.

Here, we report a new superconductor Ce_5CoGe_2 , which corresponds to a novel setting for superconductivity in proximity to magnetism. At ambient pressure, Ce_5CoGe_2 is a Kondo lattice compound showing the coexistence of ferromagnetism and cluster glass behavior below the Curie temperature (T_C) of 10.9 K (Extended Data Fig. 1) [31]. The resulting temperature-pressure phase diagram is shown schematically in Fig. 1d, where under pressure the FM order first gives way to AFM order. With further increasing pressure, the AFM order is continuously suppressed and vanishes at an AFM QCP. Interestingly, superconductivity does not emerge immediately upon the suppression of antiferromagnetic order, but appears at higher pressures, being separated from the AFM instability.

In order to track the evolution of the magnetic ground state of Ce_5CoGe_2 with pressure, the temperature dependence of the ac magnetic susceptibility was measured under pressure, and the real part $\chi'(T)$ is displayed in Fig. 2a under pressures up to 2.1 GPa. With increasing pressure, the peak in $\chi'(T)$ corresponding to the magnetic transition shifts from 9.7 K at ambient pressure to 1.7 K at 2.1 GPa, demonstrating a pressure induced suppression of magnetic order. Meanwhile, measurements in applied magnetic fields (Figs. 2b-d) reveal distinct changes in the magnetic ground state under pressure. At lower pressures such as 0.7 GPa, the transition moves to higher temperatures with increasing field, in line with a ferromagnetic transition, while at 1.8 GPa, the transition shifts to lower temperatures, which is characteristic of AFM order. At the intermediate pressure of 1.2 GPa, two peaks are observed with different field dependences, indicating the coexistence of FM ($T_C \approx 4.3$ K)

and AFM ($T_N \approx 3.5$ K) transitions at this pressure. Furthermore, the frequency dependence of $\chi'(T)$ indicates that the spin-cluster behavior present at ambient pressure [31] vanishes within the AFM phase (Extended Data Fig. 2). These results suggest that upon applying pressure to Ce_5CoGe_2 there is a change from an FM to AFM magnetic ground state. The nature of the coexistence of FM and AFM at 1.2 GPa is not yet determined; it could be that the FM-AFM boundary is first order and there are coexistent macroscopic FM and AFM domains in its vicinity, or it could be there is a more microscopic coexistence, for example if the ordering on the 4 inequivalent Ce sites evolves differently with pressure.

The electrical resistivity $\rho(T)$ of Ce_5CoGe_2 is displayed in Fig. 3a and Extended Data Fig. 3. Ce_5CoGe_2 exhibits a more metallic behavior as the pressure is increased from 0.6 GPa to 5 GPa (Extended Data Fig. 3a). The magnetic transition is also detected in the low temperature $\rho(T)$ (Fig. 3a), where the FM transition appears as a kink below which $\rho(T)$ decreases rapidly, and T_C can be defined as the position of the maximum in the derivative $d\rho(T)/dT$ (Extended Data Fig. 4). On the other hand, there is an upturn in $\rho(T)$ upon cooling below the AFM transition, and the Neel temperature T_N corresponds to the minimum in $d\rho(T)/dT$ (Extended Data Fig. 4), which could signal the opening of a gap [32]. Additional resistivity measurements in a piston–cylinder cell confirm the reproducibility of the resistivity upturn (Extended Data Fig. 5). The upturn in $\rho(T)$ moves to lower temperatures with increasing pressure, which together with the $\chi'(T)$ (Fig. 2a) and ac heat capacity results (Fig. 3b and Extended Data Fig. 6), demonstrates that the AFM transition is continuously suppressed to zero temperature, reaching a QCP at a critical pressure of $p_c \approx 3.2$ GPa. At p_c , $C_{\text{ac}}(T)/T$ diverges, while the resistivity is linear in temperature from 2 K down to at least 250 mK (Fig. 3c), indicating strange-metal behavior at the QCP. When magnetic fields are applied along the a axis, there is a change from a $\sim T$ to $\sim T^2$ dependence of $\rho(T)$, suggesting the restoration of Fermi liquid behavior in applied fields (Extended Data Fig. 7).

Figure 4a and Extended Data Fig. 3b display $\rho(T)$ at higher pressures above p_c up to 15 GPa. At 6.2 GPa, there is a sharp drop in $\rho(T)$ below 0.5 K, indicating the onset of superconductivity. At higher pressures, the transition temperature T_{sc} (determined from where $\rho(T)$ drops by 50%) moves to higher temperatures, reaching 2 K at 15 GPa, and zero-resistance is realized at lower temperatures. To corroborate the occurrence of superconductivity, ac magnetic susceptibility measurements were performed under pressure (Fig. 4b), with a small

piece of Pb in the pressure cell as a reference. The comparable jump in $\chi'(T)$ between Ce_5CoGe_2 and Pb provides clear evidence for a full shielding fraction in Ce_5CoGe_2 below the superconducting transition. Meanwhile, the normal state resistivity remains metallic across the whole pressure range, but there is a slight upturn at low temperatures (Extended Data Fig. 8), reminiscent of CeCu_2Si_2 under pressure [33].

Figure 4c displays $\rho(T)$ at 9.6 GPa under different applied magnetic fields (see also Extended Data Fig. 9 for other pressure points), while the derived upper critical fields versus temperature $B_{c2}(T)$ are shown in Fig. 4d, which are well fitted using the Werthamer-Helfand-Hohenberg (WHH) model [34]. At all pressures the upper critical field exceeds the weak coupling Pauli limit ($B_P = 1.86 T_{sc}$). For example, at 8 GPa $B_P = 1.3$ T, but the superconducting transition is still observed in applied fields above this, and an extrapolated zero-temperature value $B_{c2}(0) = 2.3$ T is obtained. The inset of Fig. 5a displays the pressure dependence of $(B'_{c2}/T_{sc})^{0.5}$, where $B'_{c2} = -(dB_{c2}/dT)_{T=T_{sc}}$ is the initial slope of the upper critical field. Within the free-electron approximation, this ratio is proportional to the relative enhancement of the effective charge-carrier mass over the free electron value, $m^*/m_0 \sim (B'_{c2}/T_{sc})^{0.5}$ [35–37]. The value of $(B'_{c2}/T_{sc})^{0.5}$, which is plotted versus T_{sc} for various heavy-fermion and other unconventional superconductors in Extended Data Fig. 10, is comparable to canonical heavy-fermion compounds such as CeIn_3 [38] and CeCoIn_5 [39]. Upon further increasing the pressure, $(B'_{c2}/T_{sc})^{0.5}$ and hence m^* decreases, reaching a value close to that of the intermediate valence superconductor PuCoIn_5 [15], as well as CeCu_2Si_2 in the high-pressure superconducting phase (Extended Data Fig. 10) [40]. In addition, although m^*/m_0 is reduced by approximately a factor of two at 14.2 GPa, it remains strongly enhanced compared with conventional BCS superconductors: m^*/m_0 in Ce_5CoGe_2 is still about 13.6 and 5.6 times larger than in MgB_2 and Nb_3Sn [41, 42], respectively (Extended Data Fig. 10). This comparison indicates that electronic correlations in Ce_5CoGe_2 are stronger than in typical conventional BCS superconductors.

The resulting temperature-pressure phase diagram of Ce_5CoGe_2 is shown in Fig. 5. The ground state evolves from FM order at ambient pressure, which changes to an AFM state above 1.2 GPa, and this antiferromagnetism is suppressed to a QCP at around $p_c \approx 3.2$ GPa. Above the QCP at 6.2 GPa, superconductivity emerges and T_{sc} increases monotonically with pressure up to at least 15 GPa. The pressure evolution of the low temperature resistivity ρ_0 is shown in Fig. 5b, where there is a pronounced peak corresponding to the FM–AFM

transition. Moreover, a broad hump in ρ_0 appears at elevated pressures after the emergence of superconductivity.

Overall these results demonstrate that Ce_5CoGe_2 manifests a new scenario for the interplay of magnetism and superconductivity, where the superconductivity emerges in proximity to a QCP associated with the suppression of AFM order, that in turn replaces the ambient pressure FM phase under pressure. While such a change of magnetic ground state occurs in several metallic ferromagnets [19], it is not typically associated with superconductivity. Moreover, unlike canonical antiferromagnetic heavy fermion superconductors [7, 37, 43, 44], the superconductivity does not appear to directly stem from a magnetic quantum critical point, but instead the superconducting dome is separate from the ordered phase (Fig. 1d), being similar to the case of $\beta\text{-YbAlB}_4$ [16, 45], suggesting that the superconductivity is not primarily driven by spin fluctuations.

Although the superconducting pairing state of Ce_5CoGe_2 is to be explored in future studies, the Coulomb repulsion associated with such a strongly correlated underlying electronic state, as evidenced by the enhanced m^* , is disfavourable to conventional s -wave superconductivity with onsite pairing. These considerations lead to the prospect that the superconductivity is driven by an alternative instability such as valence fluctuations, which are proposed to underly the high pressure superconducting dome of CeCu_2Si_2 [14, 17, 18]. An indication of the possible role of valence fluctuations in Ce_5CoGe_2 is the rapid reduction of the electronic effective mass upon increasing pressure (inset of Fig. 5a), which is characteristic of the crossover from a heavy fermion to a intermediate valence state [17]. In addition, valence fluctuations may enhance ρ_0 , as seen in pressurized $\text{CeCu}_2(\text{Si}_{1-x}\text{Ge}_x)_2$ [18], and an increase of ρ_0 is also observed above 5 GPa in Ce_5CoGe_2 , concomitant with the appearance of superconductivity. Moreover, a weak upturn of the resistivity with decreasing temperature corresponding to a $-\log T$ dependence is observed in the high-pressure superconducting regimes of both Ce_5CoGe_2 and CeCu_2Si_2 [33], which is robust against magnetic fields (Extended Data Fig. 8). Although the origin is not determined, it may be attributed to unscreened magnetic moments in the mixed valence regime. We note that in candidate valence-fluctuation driven superconductors $T_{\text{sc}}(P)$ can increase over a broad pressure range without an observed maximum. For example, it has been suggested that the superconductivity of PuCoGa_5 with a record T_{sc} of 18.5 K is mediated by valence fluctuations [15], and like Ce_5CoGe_2 , the superconducting phase of PuCoGa_5 is robust, with T_{sc} changing only

slightly over a wide pressure range [46]. It will therefore be important to extend the phase diagram to higher pressures in future measurements to establish the full evolution of the superconducting phase of Ce_5CoGe_2 .

While the upper critical field exceeding the weak-coupling Pauli limit in a centrosymmetric superconductor could hint at a non-singlet pairing state, it should be noted that other effects, namely strong coupling and an effective Landé factor that diverges significantly from the free electron value, may increase the paramagnetic limiting field. Therefore, it is of particular importance to both characterize the nature of the superconducting order parameter and pairing state, and also to reveal the dynamics associated with degrees of freedom such as spin and valence fluctuations that may drive superconductivity. Furthermore, it is necessary to understand the nature of the quantum criticality of Ce_5CoGe_2 , where strange-metal behavior is only observed in a narrow pressure range close to p_c . More broadly, such a unique scenario for the interplay of ferromagnetism, antiferromagnetism and superconductivity, together with strange metal quantum criticality, positions Ce_5CoGe_2 as a promising materials platform for exploring novel types of unconventional superconductivity in proximity to magnetic instabilities.

Methods

Single crystals of Ce_5CoGe_2 were grown using a self-flux method. Cerium ingot (Alfa Aesar, 99.9%), cobalt slug (Alfa Aesar, 99.95%), and germanium granules (PrMat, 99.9999%) were first arc-melted in a molar ratio of 9:3:1 under a titanium-gettered argon atmosphere. The obtained ingot was then placed in a tantalum crucible and sealed in an evacuated quartz tube. The tube was heated to 1150 °C, held at this temperature for 24 hours, and then slowly cooled to 550 °C.

Measurements under applied pressures up to 2.3 GPa were performed using a piston-cylinder-type pressure cell with Daphne 7373 as the pressure-transmitting medium. The applied pressure was determined from the shift in T_{sc} of a high-quality Pb single crystal [47]. Measurements at pressures up to 15 GPa were carried out in a diamond anvil cell (DAC), where Daphne 7373 was used as the pressure-transmitting medium. The DAC was loaded together with several small ruby balls for pressure determination at room temperature using the ruby fluorescence method [48]. Electrical resistance measurements in both the piston-cylinder and diamond anvil cells were performed using a standard four-probe method, with Au-wires glued to the samples using silver conductive paste. The heat capacity measurement under pressure was performed using an ac calorimetric technique, in which a heater glued onto the sample generates a small temperature oscillation ΔT by applying an ac current, and a chromel–AuFe (0.07%) thermocouple glued to the opposite side senses an ac voltage signal proportional to ΔT . The ac magnetic susceptibility measurements in a piston-cylinder-type pressure cell were carried out using an in-house-designed coil system consisting of a drive coil, a pick-up coil, and a compensation coil. The system was driven by an applied current of 0.1 mA at a frequency of 1523 Hz, and the voltage signal was detected using an SR-830 lock-in amplifier. Additional ac susceptibility measurements in a diamond anvil cell were performed up to 14 GPa using a microcoil setup. The pickup microcoil was wound from enameled Cu wire into a coil of radius of 180 μm , and positioned to maximize coupling to the sample in the sample chamber. A compensation coil was wound in the opposite direction outside the pickup coil to reduce background signals. The drive coil was placed on the gasket and wound using a 45 μm diameter enameled wire with 250 turns. A small piece of lead (Pb), with a volume approximately one-third of the sample, was included in the pressure cell as a reference. The resistance, ac magnetic susceptibility, and ac heat capacity were measured using a Teslatron-PT system equipped with an Oxford ^3He refrigerator and

a Quantum Design Physical Property Measurement System (PPMS).

Acknowledgments We acknowledge fruitful discussions with Chao Cao, Yang Liu and Piers Coleman. Work at Zhejiang University was supported by the National Key R&D Program of China (Grant No. 2022YFA1402200, 2023YFA1406303), the National Science Foundation of China (12034017, W2511006, 12494592, 1222410, 12174332). This work has been supported by the New Cornerstone Science Foundation.

Additional information Correspondence and requests for materials should be addressed to H. Q. Yuan (hqyuan@zju.edu.cn).

Author contributions H.Y. conceived the project. The crystals were grown by J.Z., Y.L, and Y.Z.. Measurements of electrical resistivity, ac susceptibility, and ac specific heat under pressure were performed by Y.Z., D.S., K.Y., and Y.H.. The experimental data were analyzed by Y.Z., D.S., Z.S., L.J., M.S., and H.Y.. Y.Z., M.S., F.S., L.J., Y.L., and H.Y. wrote the paper with input from all authors. All authors participated in discussions.

Competing financial interests The authors declare no competing financial interests.

- [1] Pfleiderer, C. Superconducting phases of *f*-electron compounds. *Rev. Mod. Phys.* **81**, 1551–1624 (2009). URL <https://link.aps.org/doi/10.1103/RevModPhys.81.1551>.
- [2] Lee, P. A., Nagaosa, N. & Wen, X.-G. Doping a Mott insulator: Physics of high-temperature superconductivity. *Reviews of Modern Physics* **78**, 17–85. URL <https://link.aps.org/doi/10.1103/RevModPhys.78.17>.
- [3] Dai, P. Antiferromagnetic order and spin dynamics in iron-based superconductors. *Rev. Mod. Phys.* **87**, 855–896 (2015). URL <https://link.aps.org/doi/10.1103/RevModPhys.87.855>.
- [4] Lang, M. & Müller, J. *Organic Superconductors*, 453–554 (Springer Berlin Heidelberg, Berlin, Heidelberg, 2004). URL https://doi.org/10.1007/978-3-642-18914-2_7.
- [5] Scalapino, D. J. A common thread: The pairing interaction for unconventional superconductors. *Rev. Mod. Phys.* **84**, 1383–1417 (2012). URL <https://link.aps.org/doi/10.1103/RevModPhys.84.1383>.
- [6] Stewart, G. R. Unconventional superconductivity. *Advances in Physics* **66**, 75–196 (2017). URL <https://doi.org/10.1080/00018732.2017.1331615>.

[7] Mathur, N. D. *et al.* Magnetically mediated superconductivity in heavy fermion compounds. *Nature* **394**, 39–43 (1998). URL <http://dx.doi.org/10.1038/27838>.

[8] Schröder, A. *et al.* Onset of antiferromagnetism in heavy-fermion metals. *Nature* **407**, 351–355 (2000). URL <http://dx.doi.org/10.1038/35030039>.

[9] Stewart, G. R. Non-Fermi-liquid Behavior in *d*- and *f*-Electron Metals. *Reviews of Modern Physics* **73**, 797–855 (2001). URL <https://link.aps.org/doi/10.1103/RevModPhys.73.797>.

[10] v. Löhneysen, H., Rosch, A., Vojta, M. & Wölfle, P. Fermi-Liquid Instabilities at Magnetic Quantum Phase Transitions. *Reviews of Modern Physics* **79**, 1015–1075 (2007). URL <https://link.aps.org/doi/10.1103/RevModPhys.79.1015>.

[11] Gegenwart, P., Si, Q. & Steglich, F. Quantum criticality in heavy-fermion metals. *Nature Physics* **4**, 186–197 (2008). URL <http://dx.doi.org/10.1038/nphys892>.

[12] Smidman, M. *et al.* Colloquium: Unconventional fully gapped superconductivity in the heavy-fermion metal CeCu_2Si_2 . *Rev. Mod. Phys.* **95**, 031002 (2023). URL <https://link.aps.org/doi/10.1103/RevModPhys.95.031002>.

[13] Sakai, A., Kuga, K. & Nakatsuji, S. Superconductivity in the Ferroquadrupolar State in the Quadrupolar Kondo Lattice $\text{PrTi}_2\text{Al}_{20}$. *Journal of the Physical Society of Japan* **81**, 083702 (2012). URL <http://dx.doi.org/10.1143/JPSJ.81.083702>.

[14] Yuan, H. Q. *et al.* Observation of Two Distinct Superconducting Phases in CeCu_2Si_2 . *Science* **302**, 2104–2107 (2003). URL <https://www.science.org/doi/abs/10.1126/science.1091648>.

[15] Bauer, E. D. *et al.* Localized 5f electrons in superconducting PuCoIn_5 : consequences for superconductivity in PuCoGa_5 . *Journal of Physics: Condensed Matter* **24**, 052206 (2011). URL <http://dx.doi.org/10.1088/0953-8984/24/5/052206>.

[16] Matsumoto, Y. *et al.* Quantum Criticality Without Tuning in the Mixed Valence Compound $\beta\text{-YbAlB}_4$. *Science* **331**, 316–319 (2011). URL <http://dx.doi.org/10.1126/science.1197531>.

[17] Yuan, H. Q. *et al.* Non-fermi liquid states in the pressurized $\text{CeCu}_2(\text{Si}_{1-x}\text{Ge}_x)_2$ system: Two critical points. *Phys. Rev. Lett.* **96**, 047008 (2006). URL <https://link.aps.org/doi/10.1103/PhysRevLett.96.047008>.

[18] Holmes, A. T., Jaccard, D. & Miyake, K. Signatures of valence fluctuations in CeCu_2Si_2 under

high pressure. *Phys. Rev. B* **69**, 024508 (2004). URL <https://link.aps.org/doi/10.1103/PhysRevB.69.024508>.

[19] Brando, M., Belitz, D., Grosche, F. M. & Kirkpatrick, T. R. Metallic quantum ferromagnets. *Rev. Mod. Phys.* **88**, 025006 (2016). URL <https://link.aps.org/doi/10.1103/RevModPhys.88.025006>.

[20] Saxena, S. S. *et al.* Superconductivity on the border of itinerant-electron ferromagnetism in UGe_2 . *Nature* **406**, 587–592 (2000). URL <http://dx.doi.org/10.1038/35020500>.

[21] Aoki, D. *et al.* Coexistence of superconductivity and ferromagnetism in URhGe . *Nature* **413**, 613–616 (2001). URL <http://dx.doi.org/10.1038/35098048>.

[22] Slooten, E., Naka, T., Gasparini, A., Huang, Y. K. & de Visser, A. Enhancement of Superconductivity near the Ferromagnetic Quantum Critical Point in UCoGe . *Phys. Rev. Lett.* **103**, 097003 (2009). URL <https://link.aps.org/doi/10.1103/PhysRevLett.103.097003>.

[23] Shen, B. *et al.* Strange-metal behaviour in a pure ferromagnetic Kondo lattice **579**, 51–55 (2020). URL <https://www.nature.com/articles/s41586-020-2052-z>.

[24] Wang, A. *et al.* Localized 4f-electrons in the quantum critical heavy fermion ferromagnet CeRh_6Ge_4 . *Science Bulletin* **66**, 1389–1394 (2021). URL <http://dx.doi.org/10.1016/j.scib.2021.03.006>.

[25] Steppke, A. *et al.* Ferromagnetic Quantum Critical Point in the Heavy-Fermion Metal $\text{YbNi}_4(\text{P}_{1-x}\text{As}_x)_2$. *Science* **339**, 933–936 (2013). URL <https://www.science.org/doi/10.1126/science.1230583>.

[26] Süllow, S., Aronson, M. C., Rainford, B. D. & Haen, P. Doniach Phase Diagram, Revisited: From Ferromagnet to Fermi Liquid in Pressurized CeRu_2Ge_2 . *Physical Review Letters* **82**, 2963–2966 (1999). URL <https://link.aps.org/doi/10.1103/PhysRevLett.82.2963>.

[27] Sidorov, V. A. *et al.* Magnetic phase diagram of the ferromagnetic Kondo-lattice compound CeAgSb_2 up to 80 kbar. *Phys. Rev. B* **67**, 224419 (2003). URL <https://link.aps.org/doi/10.1103/PhysRevB.67.224419>.

[28] Lengyel, E. *et al.* Avoided ferromagnetic quantum critical point in CeRuPO . *Phys. Rev. B* **91**, 035130 (2015). URL <https://link.aps.org/doi/10.1103/PhysRevB.91.035130>.

[29] Brando, M. *et al.* Logarithmic Fermi-Liquid Breakdown in NbFe_2 . *Phys. Rev. Lett.* **101**, 026401 (2008). URL <https://link.aps.org/doi/10.1103/PhysRevLett.101.026401>.

[30] Taufour, V. *et al.* Ferromagnetic Quantum Critical Point Avoided by the Appearance of

Another Magnetic Phase in LaCrGe_3 under Pressure. *Phys. Rev. Lett.* **117**, 037207 (2016). URL <https://link.aps.org/doi/10.1103/PhysRevLett.117.037207>.

[31] Su, D. et al. Coexistence of ferromagnetism and cluster glass behavior in Ce_5CoGe_2 . *Phys. Rev. B* **110**, 144432 (2024). URL <https://link.aps.org/doi/10.1103/PhysRevB.110.144432>.

[32] Luo, Y. et al. Pressure-tuned Quantum Criticality in the Antiferromagnetic Kondo Semimetal $\text{CeNi}_{2-\delta}\text{As}_2$. *Proceedings of the National Academy of Sciences* **112**, 13520–13524 (2015). URL <http://dx.doi.org/10.1073/pnas.1509581112>.

[33] Yuan, H. Q. Ph.D. thesis. Ph.D. thesis, Technische Universität Dresden (2003).

[34] Werthamer, N. R., Helfand, E. & Hohenberg, P. C. Temperature and Purity Dependence of the Superconducting Critical Field, H_{c2} . iii. Electron Spin and Spin-Orbit Effects. *Phys. Rev.* **147**, 295–302 (1966). URL <https://link.aps.org/doi/10.1103/PhysRev.147.295>.

[35] Knebel, G., Aoki, D., Brison, J.-P. & Flouquet, J. The quantum critical point in CeRhIn_5 : A resistivity study. *Journal of the Physical Society of Japan* **77**, 114704 (2008).

[36] Park, T., Graf, M. J., Boulaevskii, L., Sarrao, J. L. & Thompson, J. D. Electronic duality in strongly correlated matter. *Proceedings of the National Academy of Sciences* **105**, 6825–6828 (2008). URL <https://doi.org/10.1073/pnas.0801873105>.

[37] Squire, O. P. et al. Superconductivity beyond the conventional pauli limit in high-pressure CeSb_2 . *Phys. Rev. Lett.* **131**, 026001 (2023). URL <https://link.aps.org/doi/10.1103/PhysRevLett.131.026001>.

[38] Knebel, G., Braithwaite, D., Canfield, P. C., Lapertot, G. & Flouquet, J. Electronic properties of CeIn_3 under high pressure near the quantum critical point. *Phys. Rev. B* **65**, 024425 (2001). URL <https://link.aps.org/doi/10.1103/PhysRevB.65.024425>.

[39] Tayama, T. et al. Unconventional heavy-fermion superconductor CeCoIn_5 : dc magnetization study at temperatures down to 50 mK. *Phys. Rev. B* **65**, 180504 (2002). URL <https://link.aps.org/doi/10.1103/PhysRevB.65.180504>.

[40] Vargo, E., Jaccard, D., Genoud, J., Brison, J. & Flouquet, J. Upper critical field of CeCu_2Si_2 at very high pressure. *Solid State Communications* **106**, 631–636 (1998). URL [http://dx.doi.org/10.1016/S0038-1098\(98\)00086-6](http://dx.doi.org/10.1016/S0038-1098(98)00086-6).

[41] Askerzade, I. N., Gencer, A. & Güçlü, N. On the ginzburg-landau analysis of the upper critical field dHc_2 in MgB_2 . *Superconductor Science and Technology* **15**, L13–L16 (2002). URL

<http://dx.doi.org/10.1088/0953-2048/15/2/102>.

- [42] Guritanu, V. *et al.* Specific heat of Nb_3Sn : The case for a second energy gap. *Phys. Rev. B* **70**, 184526 (2004). URL <https://link.aps.org/doi/10.1103/PhysRevB.70.184526>.
- [43] Park, T. *et al.* Hidden Magnetism and Quantum Criticality in the Heavy Fermion Superconductor CeRhIn_5 **440**, 65–68 (2006). URL <https://www.nature.com/articles/nature04571>.
- [44] Schuberth, E. *et al.* Emergence of superconductivity in the canonical heavy-electron metal YbRh_2Si_2 . *Science* **351**, 485–488 (2016). URL <http://dx.doi.org/10.1126/science.aaa9733>.
- [45] Tomita, T., Kuga, K., Uwatoko, Y. & Nakatsuji, S. Pressure-induced magnetic transition exceeding 30 k in the Yb-based heavy-fermion β - YbAlB_4 . *Phys. Rev. B* **94**, 245130 (2016). URL <https://link.aps.org/doi/10.1103/PhysRevB.94.245130>.
- [46] Griveau, J.-C., Pfleiderer, C., Boulet, P., Rebizant, J. & Wastin, F. Pressure dependence of the superconductivity in PuCoGa_5 . *Journal of Magnetism and Magnetic Materials* **272–276**, 154–155 (2004). URL <http://dx.doi.org/10.1016/j.jmmm.2003.11.056>.
- [47] Eiling, A. & Schilling, J. S. Pressure and temperature dependence of electrical resistivity of Pb and Sn from 1–300 K and 0–10 GPa-use as continuous resistive pressure monitor accurate over wide temperature range; superconductivity under pressure in Pb, Sn and In. *Journal of Physics F: Metal Physics* **11**, 623 (1981). URL <https://dx.doi.org/10.1088/0305-4608/11/3/010>.
- [48] Mao, H. K., Xu, J. & Bell, P. M. Calibration of the ruby pressure gauge to 800 kbar under quasi-hydrostatic conditions. *Journal of Geophysical Research: Solid Earth* **91**, 4673–4676 (1986). URL <https://agupubs.onlinelibrary.wiley.com/doi/abs/10.1029/JB091iB05p04673>.

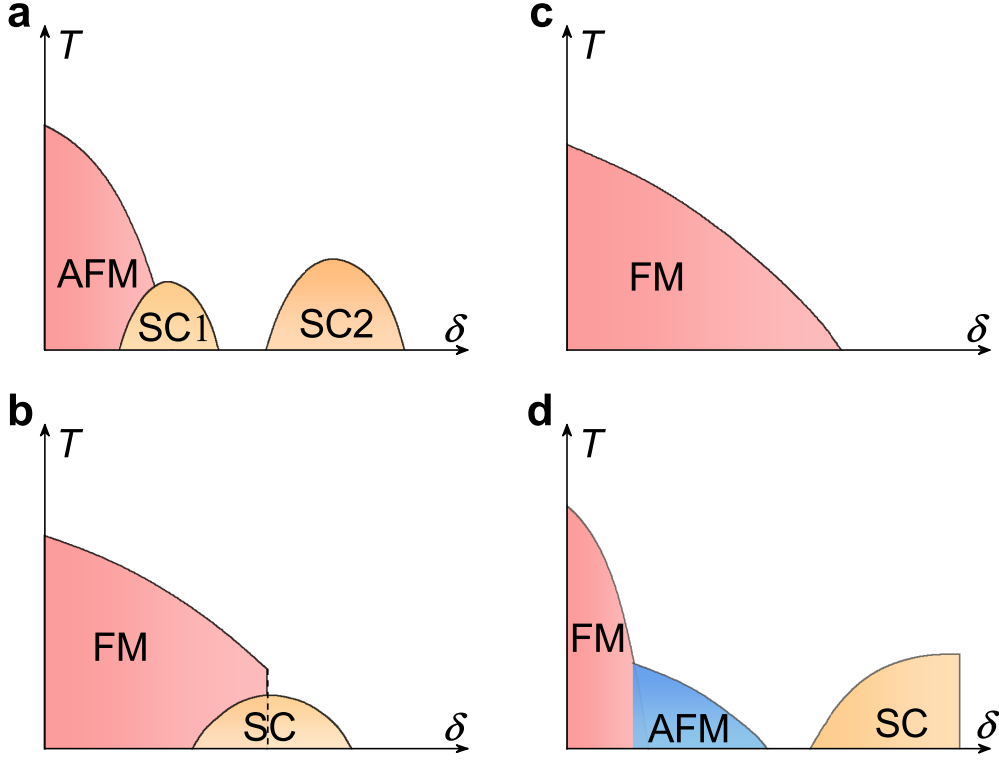


FIG. 1. Schematic phase diagrams of superconductivity and magnetism in different quantum materials. **a**, Representative phase diagram of CeCu_2Si_2 , where the first superconducting dome (SC1) emerges near the antiferromagnetic (AFM) quantum critical point (QCP). As the tuning parameter δ increases, a second superconducting dome (SC2) appears, likely driven by valence fluctuations [14, 17]. **b**, Schematic phase diagram of uranium-based ferromagnetic superconductors, where superconductivity (SC) coexists with ferromagnetic (FM) order. In these systems, the FM transition is typically first-order, avoiding a QCP [20]. **c**, Schematic phase diagram of a continuous FM QCP, at which superconductivity is not yet observed [23, 25]. **d**, Schematic phase diagram of Ce_5CoGe_2 under pressure. With increasing pressure, FM order first gives way to AFM order, which is subsequently continuously suppressed to zero temperature at an AFM QCP. Superconductivity emerges at higher pressures beyond the AFM QCP.

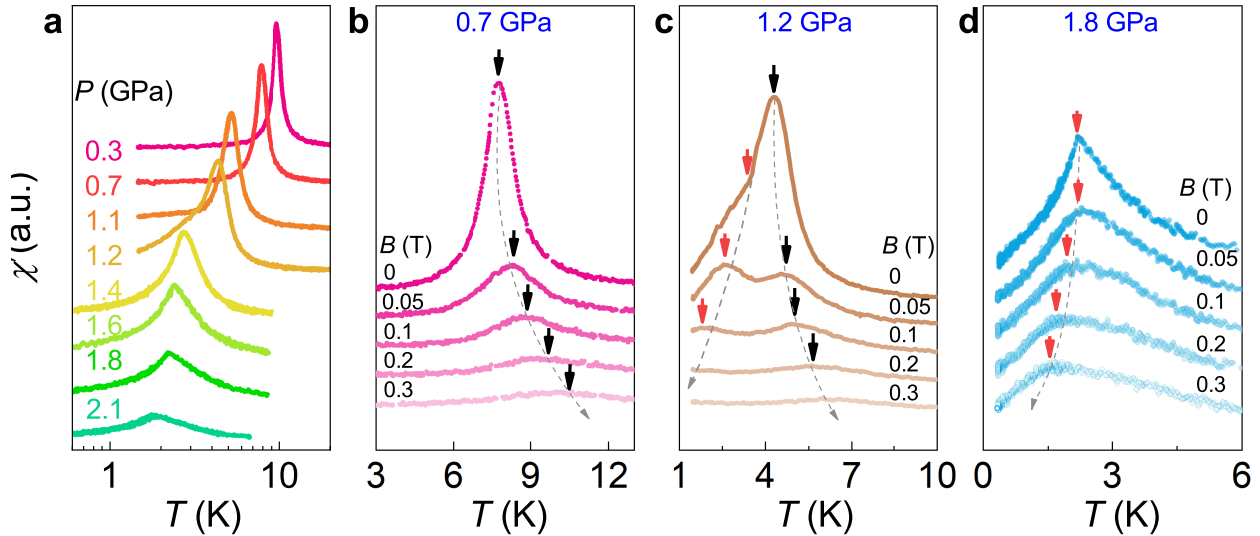


FIG. 2. **Pressure-induced FM to AFM transition in Ce_5CoGe_2 .** **a**, Temperature dependence of the real part of the ac susceptibility $\chi'(T)$ of Ce_5CoGe_2 under various pressures from 0.3 to 2.1 GPa. $\chi'(T)$ of Ce_5CoGe_2 is displayed for **b**, 0.7 GPa, **c**, 1.2 GPa, and **d**, 1.8 GPa, under various applied magnetic fields up to 0.3 T. The black and red arrows indicate FM and AFM transitions, respectively. Note that the curves are vertically shifted for clarity.

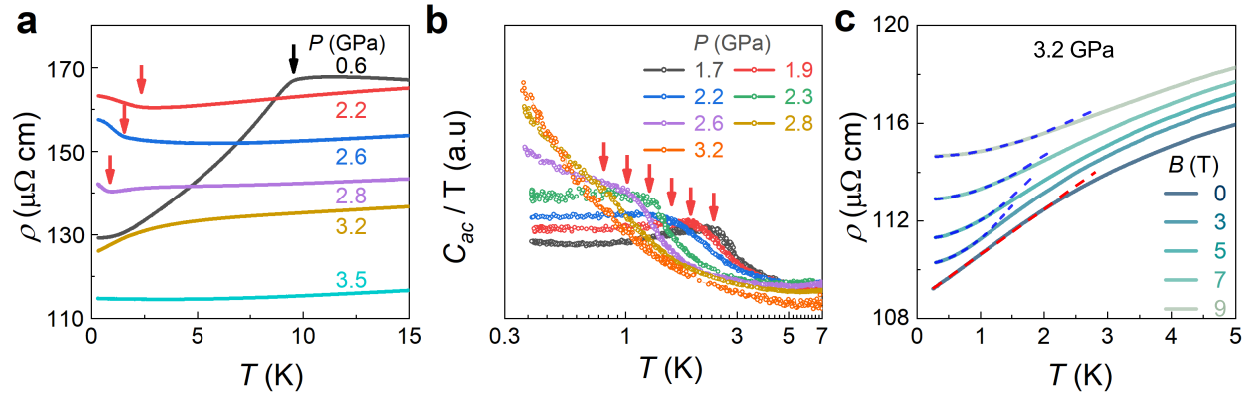


FIG. 3. **Quantum critical behavior in Ce₅CoGe₂.** **a**, Low temperature dependence of resistivity $\rho(T)$ of Ce₅CoGe₂ measured at pressures between 0.6 and 3.5 GPa. The red and black arrows indicate AFM and FM transitions, respectively. **b**, Temperature dependence of the ac heat capacity coefficient $C_{\text{ac}}(T)/T$ of Ce₅CoGe₂ measured at pressures between 1.7 and 3.2 GPa, where the red arrows indicate AFM transitions. **c**, $\rho(T)$ under various applied magnetic fields at 3.2 GPa. The red dashed line marks the T -linear resistivity, corresponding to strange-metal behavior. The blue dashed lines show fits to a T^2 dependence, corresponding to Fermi liquid behavior.

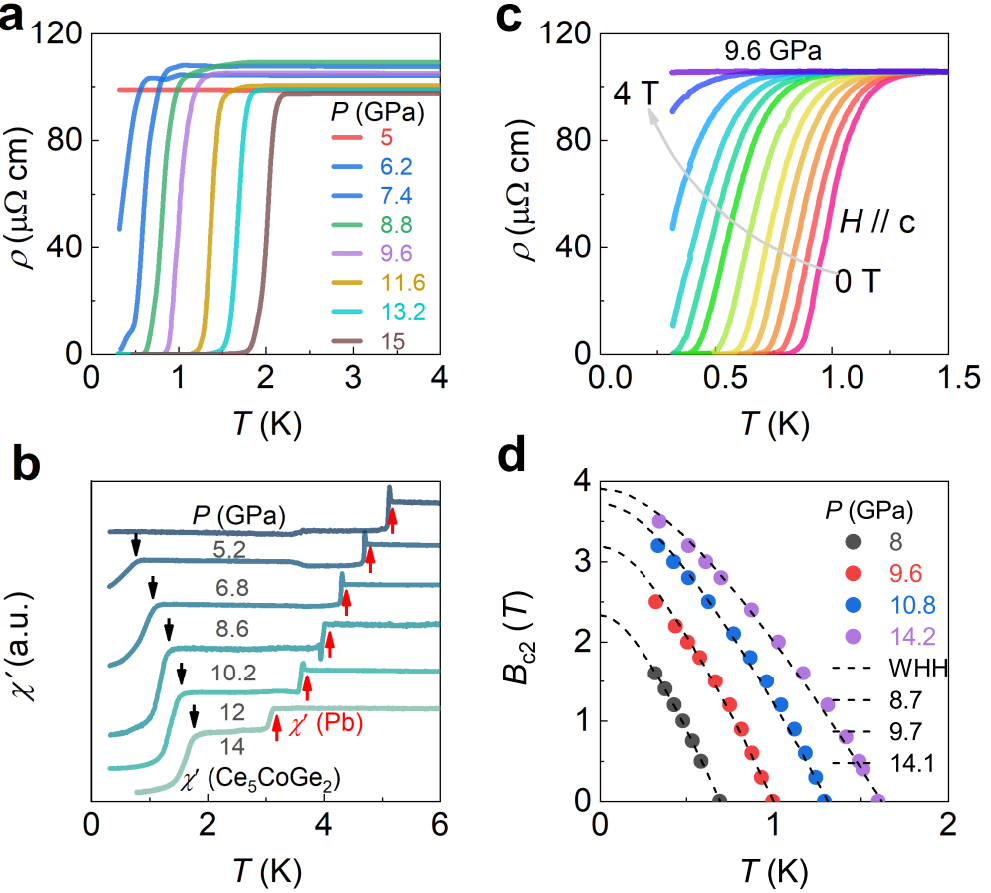


FIG. 4. Superconductivity of Ce_5CoGe_2 . **a**, Low temperature $\rho(T)$ of Ce_5CoGe_2 between 5 and 15 GPa. **b**, $\chi'(T)$ of Ce_5CoGe_2 at different pressures, where superconducting transitions corresponding to the sample and a Pb piece for reference are marked by black and red arrows, respectively. **c**, $\rho(T)$ under various applied magnetic fields at 9.6 GPa. **d**, Temperature dependence of the upper critical fields (B_{c2}) at different pressures, with black dashed lines representing the W HH model fits.

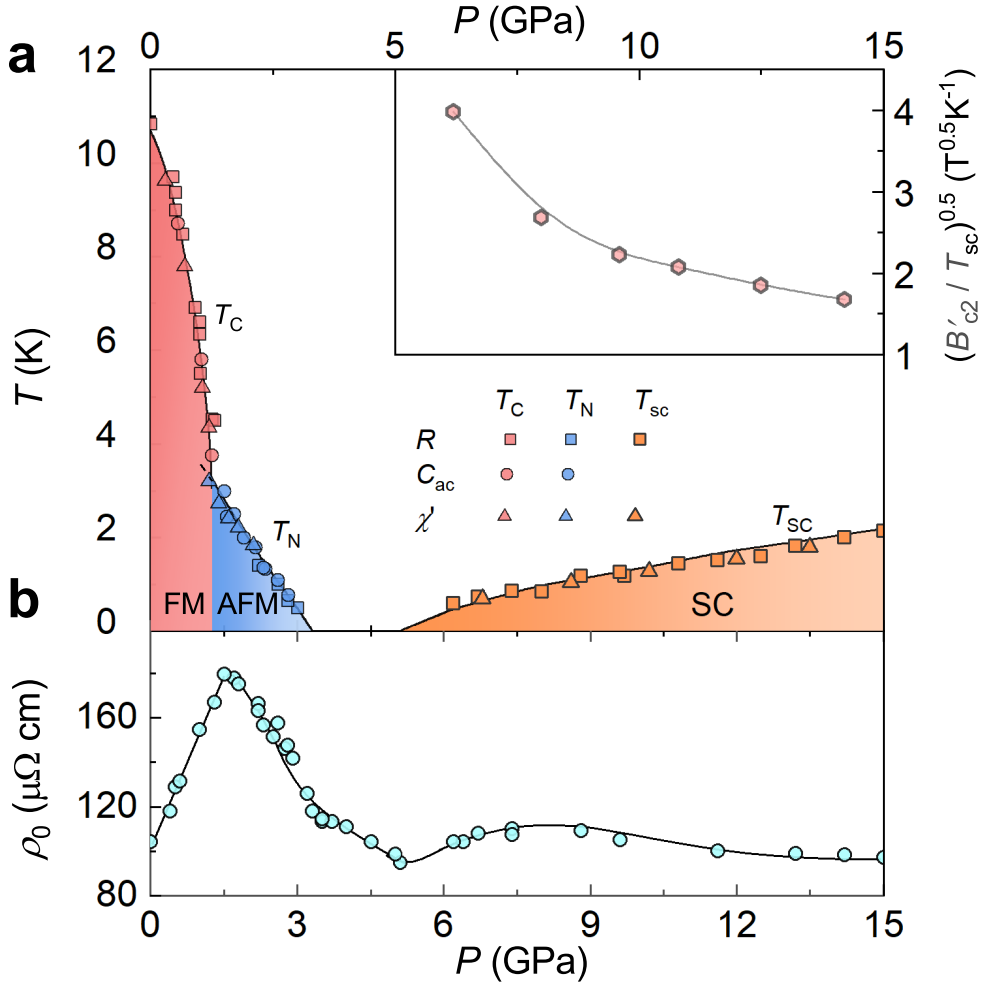


FIG. 5. Phase diagram of Ce_5CoGe_2 under pressure. **a**, Temperature–pressure phase diagram of Ce_5CoGe_2 based on resistivity, ac heat capacity, and ac susceptibility measurements. The pink, blue, and orange symbols represent T_{C} , T_{N} , and T_{sc} , respectively. The shaded regions correspond to the different labeled phases. The inset shows the pressure dependence of $(B'_{\text{c}2}/T_{\text{sc}})^{0.5}$, which qualitatively describes the evolution of the effective carrier mass. **b**, Pressure dependence of the low-temperature resistivity ρ_0 , where ρ_0 is defined as the resistivity at 0.3 K. For pressures at which superconductivity occurs, ρ_0 corresponds to the resistivity of the normal state just above the superconducting transition.